Korean J. Chem. Eng., 37(9), 1616-1622 (2020)
DOI: 10.1007/s11814-020-0563-9

pISSN: 0256-1115
eISSN: 1975-7220

ZnO/conducting polymer bilayer via sequential spin-coating for enhanced UV sensing

Taehyun Park*, Hyung Wook Choi, and Jaehyun Hur*,†**

*Department of Chemical and Biological Engineering, Gachon University, Seongnam, Gyeonggi 13120, Korea
**Department of Electrical Engineering, Gachon University,
1342 Seongnam Daero, Sujeong-gu, Seongnam-si, Gyeonggi-do 13120, Korea
(*Received 28 August 2019 • Revised 18 March 2020 • Accepted 30 April 2020*)

Abstract−Zinc oxide (ZnO) has been widely investigated as an important ultraviolet (UV) sensing material in view of its wide band gap (~3.4 eV). However, the fabrication of continuous thin films of ZnO generally requires complex, time-consuming, and expensive processes, such as sputtering and atomic layer deposition. Herein, we demonstrate a bilayer film consisting of a conducting polymer and ZnO nanoparticles sequentially deposited using a simple, rapid, and inexpensive two-step spin-coating process. In this approach, it is not necessary to have a continuous ZnO nanoparticle film as the active layer, because the conducting polymer deposited under the ZnO nanoparticles acts as a conductive and continuous supporting layer for the particles. Poly(3,4-ethylenedioxythiophene) : polystyrene sulfonate (PEDOT : PSS) is used as the auxiliary layer to promote the efficient transport of photo-carriers generated from ZnO nanoparticles under UV light. As a result, under UV light (365 nm), photocurrents obtained from a ZnO/PEDOT : PSS bilayer film are significantly higher (~20 times) than that from a ZnO layer for a given voltage bias. The photoelectric performance can be further tuned by controlling the speed of spin-coating in the deposition of ZnO nanoparticles. The stability and photo response (rise and decay time) of the ZnO/PEDOT : PSS bilayer film under the repeated on-off condition are also reported.

Keywords: Zinc Oxide Nanoparticles, PEDOT : PSS, Bilayer, Spin Coating, UV Sensor

INTRODUCTION

Ultraviolet (UV) sensors have drawn a great deal of attention due to their potential applications in various fields including environmental monitoring, flame warning, biological sensors, and space communication [1-6]. ZnO has been extensively studied for its application as an excellent active material for UV sensors because of its intrinsic wavelength selectivity (or visible-blindness) associated with its wide direct bandgap (3.4 eV) at room temperature [7-11]. More specifically, a ZnO nanoparticle (NP) layer can be a good alternative to ZnO thin films that require complicated and expensive vacuum processes for their fabrication. UV sensors using ZnO NPs are preferred for the following reasons: i) ZnO NP films can be formed using simple and inexpensive solution-based processes (e.g., spin-coating), ii) enhanced sensitivity can be achieved due to the high surface-to-volume ratio, and iii) it is relatively easy to control ZnO NP morphology. With this aim, many studies have reported on the application of ZnO NPs as UV sensors [12,13], but most of them have focused on controlling the morphology of ZnO NPs. This approach, however, has limitations since the sensitivity and photo-response time cannot be systematically controlled and connectivity between ZnO NPs also needs to be ensured.

Progressing beyond the above-mentioned approaches, several recent studies have reported the introduction of an additional conductive layer in ZnO NP films to enhance its performance as a UV sensor [14-16]. Fundamentally, this concept is based on including a continuous layer of a conductive material in the proximity of ZnO NPs to effectively reduce the distance travelled by photocarriers between electrodes; this approach also serves to provide continuous connectivity between the ZnO NPs. However, previously mentioned studies used mostly graphene-based materials as auxiliary conducting layers which cannot be easily formed using a simple spin-coating process [14-16].

In this study, we introduce poly(3,4-ethylenedioxythiophene) polystyrene sulfonate (PEDOT : PSS) as an auxiliary conductive layer in ZnO NP-based UV sensors (a bilayer film consisting of ZnO NP and PEDOT : PSS) using a simple and facile sequential spin-coating process. PEDOT : PSS acts as a continuous conductive layer under the ZnO NPs, which effectively reduces the distance travelled by photocarriers, thus enhancing carrier transport and improving the performance (both sensitivity and photo-responsivity) of UV sensors. Furthermore, the performance of UV sensors can be tuned by controlling the spin-coating speed during the formation of the bilayer.

EXPERIMENTAL SECTION

1. Preparation of a UV Sensor Based on ZnO/PEDOT : PSS Bilayer Films

ZnO/PEDOT : PSS bilayer films were prepared by a sequential spin-coating process. Details of the device structure and the manufacturing process are described in Fig. 1. ZnO suspension was prepared by dispersing ZnO NPs (Sigma Aldrich) in ethanol at a concentration of 100 mg/ml for 2 h. The PEDOT : PSS solution (Heraeus, PVPAI4083) was mixed with isopropyl alcohol, (IPA, Sigma

†To whom correspondence should be addressed.
E-mail: jhhur@gachon.ac.kr

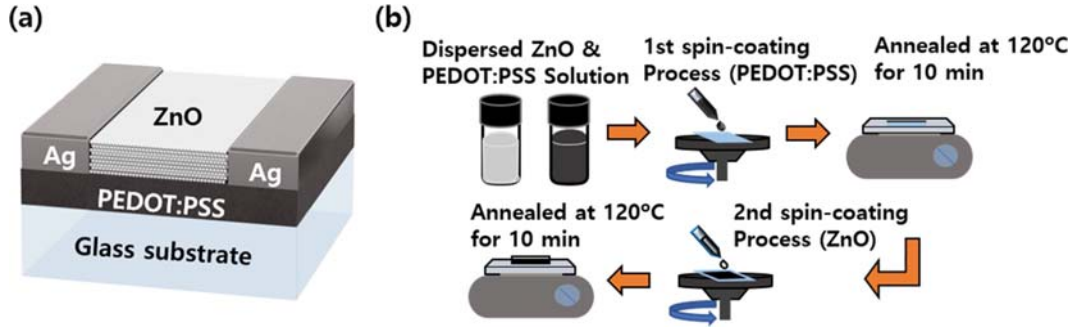

Fig. 1. (a) Device structure of ZnO/PEDOT : PSS UV sensor, and (b) schematic illustration of the deposition process for the fabrication of ZnO/PEDOT : PSS bilayer film.

Aldrich, 99.5%) in a 3 : 1 ratio (v : v) and sonicated for 1 h. A glass substrate (RnD Korea, 15×15 mm) was cleaned by washing with acetone, IPA, and distilled water, followed by drying under flowing nitrogen gas. The dried substrate was treated with UV ozone (UV SMT, 25 W) for 30 min to improve its wettability to the coating material. The substrate was first spin-coated with the PEDOT : PSS solution at 2,400 rpm for 30 s, followed by annealing at 120 °C for 10 min. Next, the ZnO solution was spin-coated at different speeds (from 500 rpm to 3,000 rpm), followed by annealing at 120 °C for 10 min. Subsequently, ZnO NPs were partially removed using a cotton swab which was wetted with ethanol that can selectively dissolve the ZnO NPs; in our separate experiment, it was confirmed that ethanol cannot dissolve PEDOT : PSS. This step was required to ensure the direct contact between top electrode and auxiliary conductive layer (PEDOT : PSS). Two electrodes (5 mm apart) were formed using silver paste (CANS, P-100). Bare ZnO NP film was also prepared in the same manner to be used as a control.

2. Characterization & Device Measurements

A UV-vis spectrophotometer (Perkin Elmer, LAMDA 750) was used to measure the optical properties of the prepared ZnO/PEDOT : PSS bilayer films. The morphology of the films was characterized by field emission scanning electron microscopy (FE-SEM, S-4700, Mono CL, Hitachi at the Smart Materials Research Center for IoT at Gachon University for its instrumental support). The particle size distribution was measured using dynamic light scattering instrument (ELS, ELS-8000, Otsuka). Current-voltage (I-V) and current-time (I-t) characteristics of the UV sensors were measured with a Keithley 2400 source meter under UV and in the dark. The light source used was a UV lamp (Minimax UV-5F) with a principal emission wavelength of 365 nm. A mechanical shutter placed below the UV light source allowed us to study the performance of the sensors under repeated on-off conditions.

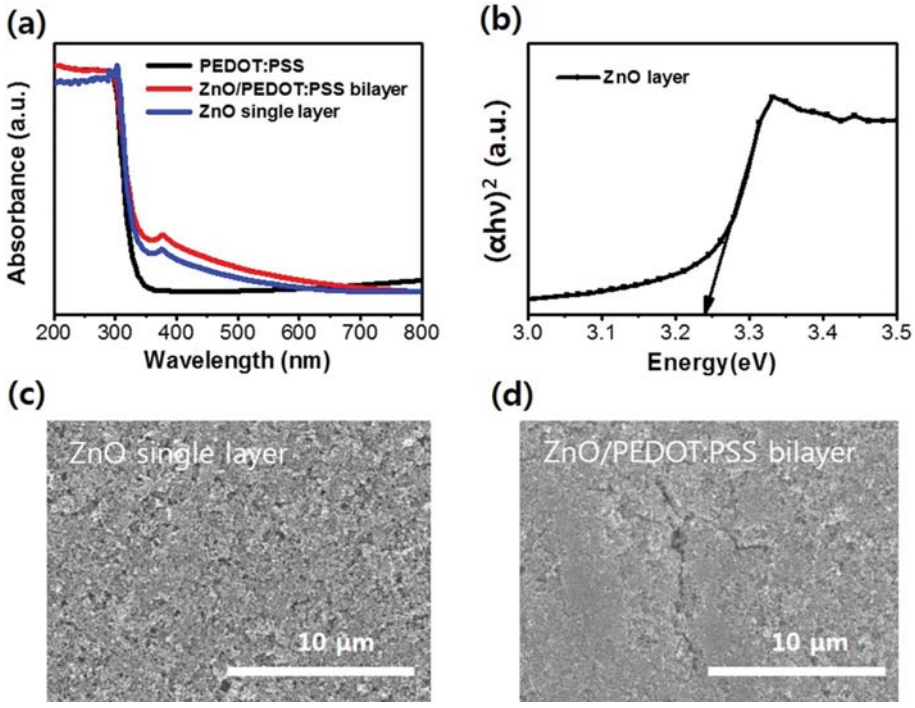

Fig. 2. (a) UV-vis absorption spectra of the ZnO single layer, ZnO/PEDOT : PSS bilayer, and PEDOT : PSS films, and (b) Tauc plot for the ZnO layer. SEM images of (c) ZnO single layer, and (d) ZnO/PEDOT : PSS bilayer.

RESULTS AND DISCUSSION

1. Characterization of ZnO and ZnO/PEDOT : PSS Bilayer Film

Fig. 2(a) presents the optical absorbance of the ZnO NP single layer and ZnO/PEDOT : PSS bilayer films. Both films consistently show selective absorption in the UVA region (315-400 nm) with maximum absorption at ~370 nm. The absorbance intensity in the UVA region for the ZnO/PEDOT : PSS bilayer is similar to that of the ZnO single layer, indicating that there is negligible reduction in absorbance due to the presence of PEDOT : PSS. This is expected since a single layer of PEDOT : PSS has negligible light absorption in the UVA region (Fig. 2(a)) and plays only a subsidiary role in the UV sensing process of the ZnO active layer. Fig. 2(b) shows that the optical band gap of the ZnO single layer film can be estimated using the Tauc relationship [17,18].

$$(\alpha h\nu)^2 = A(h\nu - E_g) \quad (1)$$

where A is a constant, h is the Planck constant, ν is the frequency of the photon, α is the absorption coefficient of the material, and E_g is the energy gap of the material. The band gap of ZnO was measured to be ~3.24 eV, corresponding to a wavelength of (~383 nm), which is in the UVA region. Fig. 2(c) and 2(d) display the morphologies of the ZnO single layer and ZnO/PEDOT : PSS bilayer films. The commercial ZnO NPs used in this study have a large size distribution (Fig. S1), and it is difficult to prepare the film with completely regular surface quality using these different sized ZnO NPs. Nevertheless, the packing density of ZnO NPs on the PEDOT : PSS (i.e., ZnO/PEDOT : PSS) film is found to be higher than that in the pure ZnO layer. This difference is ascribed to the difference in surface characteristics between glass and polymer (PEDOT : PSS). ZnO NPs tend to be more efficiently packed on the polymer than on the glass substrate despite the application of UV ozone treatment on the glass substrate. The more uniform arrangement of ZnO NP on PEDOT : PSS is expected to be favorable to increasing the photocarrier concentration under UV irradiation due to the increased surface-to-volume ratio of ZnO NPs on this surface. The film quality of ZnO NPs can be improved further if monodisperse ZnO NPs (that could be separately synthesized) are used, which remains our future study.

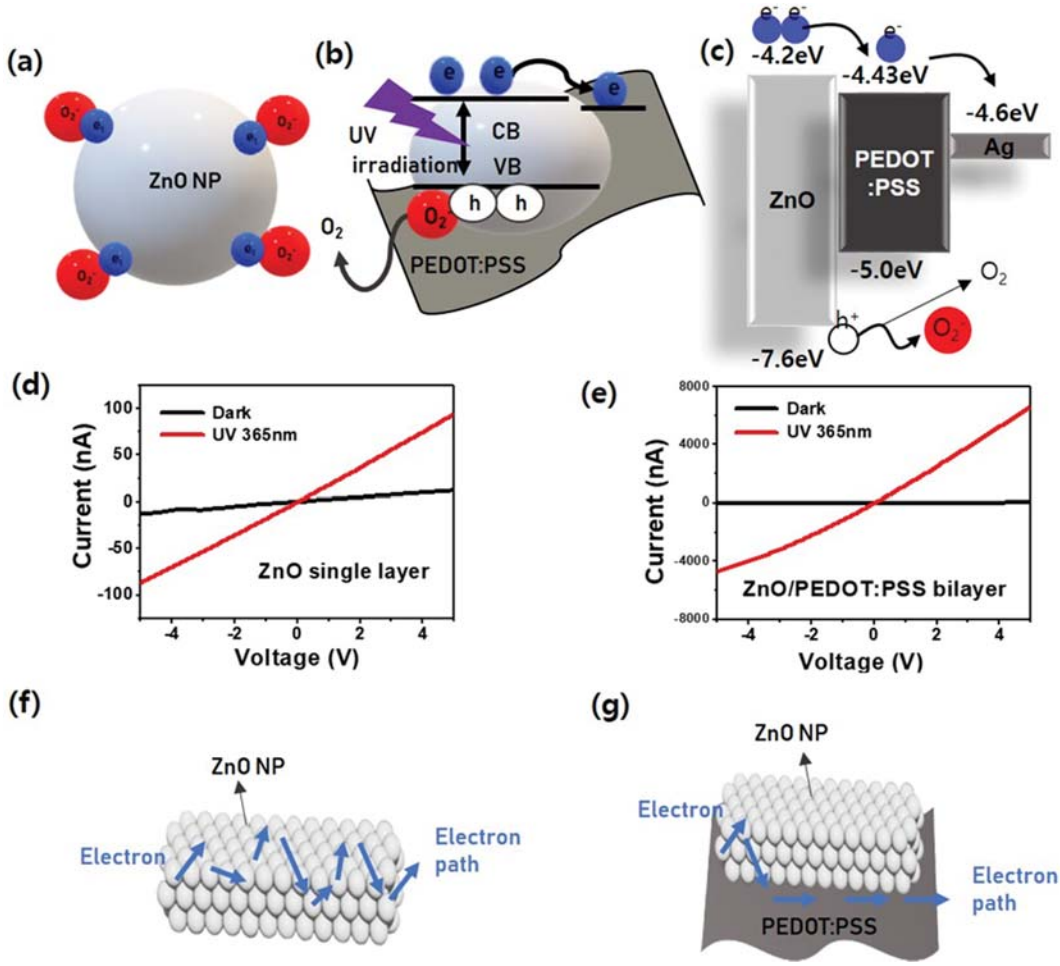

Fig. 3. Schematic illustration of the principle of photocurrent generation for (a) ZnO NP and (b) ZnO/PEDOT : PSS bilayer films. (c) Energy band structure of ZnO, PEDOT : PSS and Ag electrode. Current-voltage characteristics of (d) ZnO NP and (e) ZnO/PEDOT : PSS bilayer films under UV light (365 nm) of 0.5 mW/cm^2 intensity. Schematic illustration explaining the principle of photocarrier transport for (f) ZnO NP and (g) ZnO/PEDOT : PSS bilayer films.

2. Electrical Characteristics of ZnO Single Layer and ZnO/PEDOT : PSS Bilayer Films

The principle of photocurrent generation for ZnO NP under UV light has been established in many previous studies (Fig. 3(a) and 3(b), [19]). Briefly, when there is no external UV light source, electro-negative oxygen molecules in the atmosphere tend to combine with electrons on the ZnO surface to form negatively charged molecules (O_2^-). Upon UV irradiation, electron-hole pairs are generated inside ZnO; the holes recombine with negatively charged oxygen molecules (O_2^-) to form neutral oxygen molecules that are released into air, while the free electrons generated simultaneously act as photocarriers under the applied voltage bias between the two electrodes and contribute to increasing the electrical conductivity. These processes can be summarized as follows.

In the dark, in air:

$$O_2(g)+e^- \rightarrow O_2^-(ad) \quad (2)$$

$$O_2(g)+2e^- \rightarrow O_2^{2-}(ad) \quad (3)$$

Under UV irradiation in air:

$$ZnO \xrightarrow{UV} h^+ + e^- \quad (4)$$

$$O_2^-(ad)+h^+ \rightarrow O_2(g) \quad (5)$$

$$O_2^{2-}(ad)+2h^+ \rightarrow O_2(g) \quad (6)$$

Fig. 3(d) and 3(e) show the I-V curves for two different films under 365 nm UV irradiation with an intensity of 0.5 mW/cm^2. The sensitivity (S) of the UV sensor can be calculated using the following equation:

$$S = \frac{I_{uv} - I_d}{I_d} \times 100 \quad (7)$$

where I_{uv} and I_d refer to the currents under UV illumination and in the dark, respectively. The sensitivity of ZnO/PEDOT : PSS bilayer is found to be much higher (2.2×10^4) than that of the ZnO single layer (6.7×10^2) at 5 V bias. The enhanced sensitivity in the presence of PEDOT : PSS under the ZnO NPs can be explained as follows. In the case of a pure ZnO NP film, the only available pathway for free electrons to travel between the two electrodes is through adjacent particles. In the course of this process, considering the large distance between the two electrodes (5 mm), there is a high probability that the number of photocarriers (free electrons) is significantly diminished due to recombination with neutral oxygen molecules (O_2) in the air or with holes (h^+) in other ZnO NPs. In contrast, in the ZnO/PEDOT : PSS bilayer film, the presence of the conductive PEDOT : PSS layer limits the reduction in the number of photocarriers. This implies that the effective distance of photocarrier transport in ZnO NPs is remarkably reduced simply by introducing a conductive polymer sub-layer under the ZnO NP film. To elucidate the different mechanisms between ZnO NP single layer and ZnO NP/PEDOT : PSS bilayer, the photocurrents of these two different cases were measured under the effect of ZnO NP thickness (Fig. S2). As for the ZnO NP layer, the current level progressively increased with the increasing film thickness owing to the increased number of photocarriers that were mostly moving in the lateral direction. In the case of ZnO NP/PEDOT : PSS, when the thickness was ~500 nm, there was almost no significant difference in current level between ZnO NP layer and ZnO NP/PEDOT : PSS bilayer. However, when the thickness of the ZnO film increased to higher than 1 μm for ZnO NP/PEDOT : PSS bilayer, a current level dramatically increased (on the order of μA at 4 V bias) due to the much higher number of photocarriers generated from the thicker ZnO NP layer which were directly extracted to conductive PEDOT : PSS in the vertical direction and contributed to the current increase. However, when the ZnO NP film thickness reached as high as 3 μm in ZnO NP/PEDOT : PSS bilayer, the increased current level became insignificant compared with the case in 1 μm-thick ZnO/PEDOT : PSS bilayer film. This means that if the thickness of ZnO NP is at the reasonable level (1-3 μm) in ZnO NP/PEDOT : PSS (this high thickness has not been generally applied in other researches such as solar cells, OLED, etc.), the photocurrent can be greatly increased by increasing the thickness of ZnO NP. On the other hand, when the ZnO NP is too thick, the photocarriers generated at the top of the ZnO NP film cannot reach the bottom PEDOT : PSS layer and are prone to be lost due to the recombination inside of the ZnO NP film.

The energy band structures of the materials were considered and shown in Fig. 3(c). Normally, the LUMO level of PEDOT : PSS is higher than the conduction band minimum of ZnO, but PEDOT : PSS solution treated with IPA (like in our work) can reduce the LUMO level of deposited PEDOT : PSS film (LUMO: −4.43 eV) [20]. Therefore, the photo-generated electrons from ZnO layer can easily pass over to the PEDOT : PSS layer. Note also that the presence of PEDOT : PSS does not have any negative effect on the UV absorbance of ZnO as evidenced in Fig. 2(a) and 2(b). In addition, Fig. S3(a) and S3(b) show the deposited PEDOT : PSS layer and its current-voltage characteristics. There is no additional photogenerated current from bare PEDOT : PSS layer under the UV irradiation, but using PEDOT : PSS as an auxiliary conductive layer significantly improves the sensitivity of a ZnO NP-based UV sensor.

Fig. 4(a) and 4(b) show the photoresponsivity of the ZnO single layer along with ZnO/PEDOT : PSS bilayer films spin-coated at different coating speeds, under UV light with 365 nm wavelength and 0.5 mW/cm^2 light intensity. The spin-coating speed is an important parameter that determines the thickness of the ZnO NP layer, which in turn significantly affects the responsivity of the UV sensor. The photoresponsivity (R) of the UV sensor can be calculated using the following equation:

$$R = \frac{I_{ph}}{P} \quad (8)$$

where R is the photoresponsivity, I_{ph} is the current density, P is the power density of the light source. The photoresponsivity increases with decrease in spin-coating speed since the thickness of the ZnO NP layer generally decreases as a function of the spin-coating speed. Quantitatively, the thickness of a spin-coated film is estimated using Meyerhofer's equation [21-23].

$$h_f = \left(\frac{3\eta_o E}{2(1-C_0)\rho\omega}\right)^{\frac{1}{3}} \quad (9)$$

where h_f is the final film thickness, E is the solvent evaporation rate, ρ is the density of the solvent, ω is the angular velocity of spin-coat-

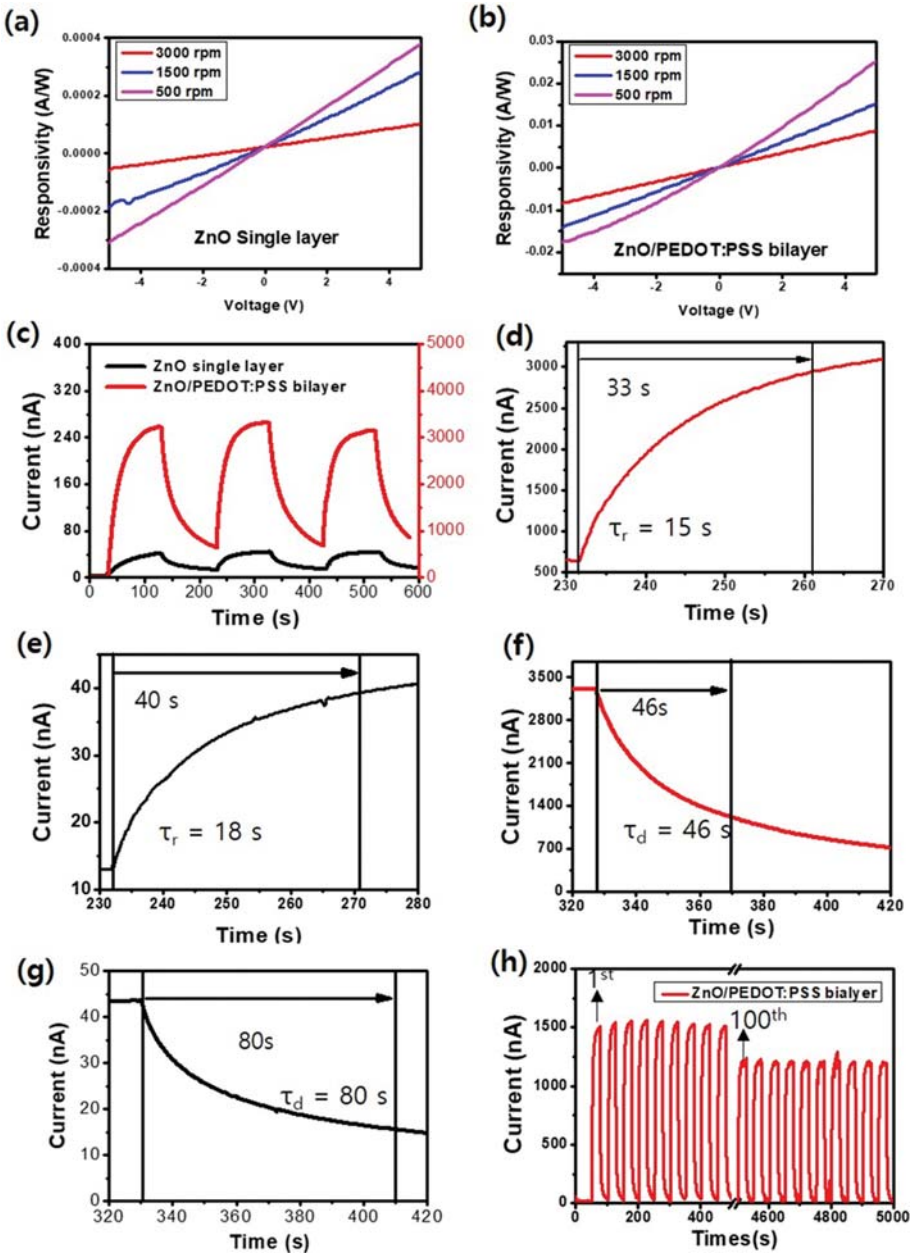

Fig. 4. Photoresponsivity of (a) ZnO NP and (b) ZnO/PEDOT : PSS bilayer films deposited at different spin-coating speeds; (c) comparison of the current-time characteristics of ZnO NP to those of the ZnO/PEDOT : PSS bilayer film under repeated UV on/off operation; rise time of (d) ZnO/PEDOT : PSS bilayer film and (e) ZnO single layer film, decay time of (f) ZnO/PEDOT : PSS bilayer film and (g) ZnO single layer film, (h) photostability of ZnO/PEDOT : PSS bilayer film during 100 cycles.

ing, C_0 is the initial concentration of the solute, and η_o is the viscosity at C_0. Given that all the parameters are constant except for ω, the film thickness is proportional to $\omega^{-2/3}$. Indeed, we observed that the photocurrent level progressively increased as the spin-coating speed was decreased from 3,000 rpm to 500 rpm.

Specifically, values of photoresponsivity for the ZnO layer were 3.8×10^{-4}, 2.8×10^{-4}, and 1.0×10^{-4} by the unit of (A/W) for the spin-coating speeds of 500, 1,500, and 3,000 rpm at 5 V bias, 0.5 mW/cm^2 of UV light intensity, 7.5×10^{-3} cm^2 of the active area, respectively (Fig. 4(a)). Further decrease in spin-coating speed (lower than 500 rpm) did not enhance the sensitivity because of poor ZnO NP film quality due to the very low coating speed as shown in Fig. S4. This trend was maintained for ZnO/PEDOT : PSS, but the photoresponsivity values were significantly enhanced to 2.5×10^{-2}, 1.5×10^{-2}, and 8.8×10^{-3} by the unit of (A/W) for spin-coating speeds of 500, 1,500, and 3,000 rpm at 5 V bias, 0.5 mW/cm^2 of UV light intensity, 7.5×10^{-3} cm^2 of the active area, respectively (Fig. 4(b)). Fig. 4(c)-4(g) show the current-time (I-t) characteristics of the ZnO single layer and ZnO/PEDOT : PSS bilayer films under UV light of 365 nm wavelength and 0.5 mW/cm^2 intensity. As shown in Fig. 4(c), the ZnO/PEDOT : PSS bilayer film shows a much higher on/off current ratio and a more stable performance than the ZnO single layer

during repeated on/off operations. Furthermore, the ZnO/PEDOT:PSS bilayer shows a much faster response than the ZnO layer. The rise time (the time to reach 90% of the maximum current) and recovery time (the time required for the maximum photocurrent to reduce by 37% after the light source is turned off) were all consistently much shorter for ZnO/PEDOT:PSS than those for the ZnO NP single layer. For quantified comparison, rise time constant (τ_r) and decay time constant (τ_d) were introduced, which can be calculated using the following equations:

$$I(t) = I_0\left(1 - e^{-\frac{t}{\tau_r}}\right) \text{ for rise time constant } (\tau_r) \quad (10)$$

$$I(t) = I_0\left(e^{-\frac{t}{\tau_d}}\right) \text{ for decay time constant } (\tau_d) \quad (11)$$

As a result, the estimated for rise/decay constants were 15/46 s for ZnO/PEDOT:PSS (Fig. 4(d) and 4(f)), and 18/80 s for ZnO (Fig. 4(e) and 4(g)). These results further demonstrate the superiority of ZnO/PEDOT:PSS bilayer as compared to the ZnO single layer; this better performance is due to the introduction of a conductive PEDOT:PSS supporting layer, which is favorable for efficient photocarrier transport. Although this rise and decay time can be relatively slow, the control of ZnO layer thickness in ZnO/PEDOT:PSS can significantly improve the photo response speed. Indeed, when we reduced the thickness of ZnO layer using highly diluted ZnO NP solution (from 0.1 g/ml to 0.01 g/ml) in spin coating, the response time could be significantly reduced from hundreds of seconds to a few seconds (Fig. S5). However, in this case, we had to obviously sacrifice the photocurrent level (or responsivity) because the response time and responsivity were in the trade-off relationship. Depending on the real applications, we can fully tune the device performance in terms of responsivity and response time by controlling the ZnO layer thickness. Fig. 4(h) represents the photostability of the ZnO/PEDOT:PSS bilayer film based UV sensor under repeated on-off conditions up to 100 cycles at 1 V bias. Although a certain level of photocurrent decrease was observed after 100 cycles, the device still showed a clear on-off behavior after 100 cycles. In our future study, the response performance and stability can be further improved by constructing a vertical-type device in which each component is deposited with layer-by-layer fashion [24]. Alternatively, the use of interdigitated electrode with much smaller electrode distance or different nanostructured ZnO can also improve the response performance given that a lateral-type device is to be fabricated [25].

CONCLUSION

We demonstrated a high-performance UV sensor based on ZnO/PEDOT:PSS bilayer prepared by a simple sequential spin-coating process. The effect of introducing a conducting polymer sub-layer under the ZnO NP layer was systematically investigated. The conducting polymer underlayer acts as an auxiliary conductive channel to effectively reduce the distance for photocarrier transport, thereby enhancing the sensitivity of the UV sensor. In addition, faster photoresponse and more stable long-term operation have been demonstrated for the ZnO/PEDOT:PSS bilayerfilm when compared with ZnO single layer films. This excellent performance makes ZnO/PEDOT:PSS-based UV sensor a promising candidate for commercial UV sensor application.

ACKNOWLEDGEMENTS

This research was supported by the Korea Electric Power Corporation (Grant number: R18XA02). This work was supported by the Korea Institute of Energy Technology Evaluation and Planning (KETEP) and the Ministry of Trade, Industry & Energy (MOTIE) of the Republic of Korea (No. 20194030202290). We thank the Smart Materials Research Center for IoT at Gachon University for its instrumental support (SEM).

SUPPORTING INFORMATION

Additional information as noted in the text. This information is available via the Internet at http://www.springer.com/chemistry/journal/11814.

REFERENCES

1. S. Zhang, L. Cai, T. Wang, R. Shi, J. Miao, L. Wei, Y. Chen, N. Sepúlveda and C. Wang, *Sci. Rep.*, **5**, 17883 (2015).
2. Y.-Q. Yu, L.-B. Luo, M.-Z. Wang, B. Wang, L.-H. Zeng, C.-Y. Wu, J.-S. Jie, J.-W. Liu, L. Wang and S.-H. Yu, *Nano Res.*, **8**, 1098 (2015).
3. A. G. Ardakani, M. Pazoki, S. M. Mahdavi, A. R. Bahrampour and N. Taghavinia, *Appl. Surf. Sci.*, **258**, 5405 (2012).
4. J. Kim, K. Y. Shin, M. H. Raza, N. Pinna and Y. E. Sung, *Korean J. Chem. Eng.*, **36**, 1157 (2019).
5. M. Farzadkia, K. Rahmani, M. Gholami, A. Esrafili, A. Rahmani and H. Rahmani, *Korean J. Chem. Eng.*, **31**, 2014 (2014).
6. Y. S. Seo and S. G. Oh, *Korean J. Chem. Eng.*, **36**, 2118 (2019).
7. K. Yu, Y. Zhang, F. Xu, Q. Li, Z. Zhu and Q. Wan, *Appl. Phys. Lett.*, **88**, 153123 (2006).
8. H. Seong, J. Yun, J. H. Jun, K. Cho and S. Kim, *Nanotechnology*, **20**, 245201 (2009).
9. Y. Liu, N. Wei, Q. Zeng, J. Han, H. Huang, D. Zhong, F. Wang, L. Ding, J. Xia and H. Xu, *Adv. Opt. Mater.*, **4**, 238 (2016).
10. X. Liu, H. Du, P. Wang, T.-T. Lim and X. W. Sun, *J. Mater. Chem. C.*, **2**, 9536 (2014).
11. D. Lin, H. Wu, W. Zhang, H. Li and W. Pan, *Appl. Phys. Lett.*, **94**, 172103 (2009).
12. S. I. Inamdar and K. Y. Rajpure, *J. Alloys Compd.*, **595**, 55 (2014).
13. K. J. Chen, F. Y. Hung, S. J. Chang and S. J. Young, *J. Alloys Compd.*, **479**, 674 (2009).
14. Z. Wang, X. Zhan, Y. Wang, S. Muhammad, Y. Huang and J. He, *Nanoscale*, **4**, 2678 (2012).
15. T. V. Tam, S. H. Hur, J. S. Chung and W. M. Choi, *Sens. Actuators, A*, **233**, 368 (2015).
16. D. I. Son, Y. H. Yang, T. W. Kim and W. I. Park, *Appl. Phys. Lett.*, **102**, 021105 (2013).
17. A. Sáenz-Trevizo, P. Amézaga-Madrid, P. Pizá-Ruiz, W. Antúnez-Flores and M. Miki-Yoshida, *Mat. Res.*, **19**, 33 (2016).
18. E. A. Davis and N. F. Mott, *Philos. Mag.*, **22**, 0903 (1970).
19. K. H. Keem, H. S. Kim, G.-T. Kim, J. S. Lee, B. D. Min, K. A. Cho,

M.-Y. Sung and S. S. Kim, *Appl. Phys. Lett.*, **84**, 4376 (2004).
20. W. Zhang, X. Bi, X. Zhao, Z. Zhao, J. Zhu, S. Dai, Y. Ku and S. Yang, *Org. Electron.*, **15**, 3445 (2014).
21. M. D. Tyona, *Adv. Mater. Res.*, **2**, 195 (2013).
22. Y. Mouhamad, P. Mokarian-Tabari, N. Clarke, R. A. L. Jones and M. Geoghegan, *J. Appl. Phys.*, **116**, 123513 (2014).
23. D. Meyerhofer, *J. Appl. Phys.*, **49**, 3993 (1978).
24. B. D. Boruah, A. Mukherjee, S. Sridhar and A. Misra, *ACS Appl. Mater. Interfaces*, **7**, 10606 (2015).
25. G. H. Shin, H. Y. Kim and J. H. Kim, *Korean J. Chem. Eng.*, **35**, 573 (2018).

Supporting Information

ZnO/conducting polymer bilayer via sequential spin-coating for enhanced UV sensing

Taehyun Park*, Hyung Wook Choi, and Jaehyun Hur*,†**

*Department of Chemical and Biological Engineering, Gachon University, Seongnam, Gyeonggi 13120, Korea
**Department of Electrical Engineering, Gachon University,
1342 Seongnam Daero, Sujeong-gu, Seongnam-si, Gyeonggi-do 13120, Korea
(*Received 28 August 2019 • Revised 18 March 2020 • Accepted 30 April 2020*)

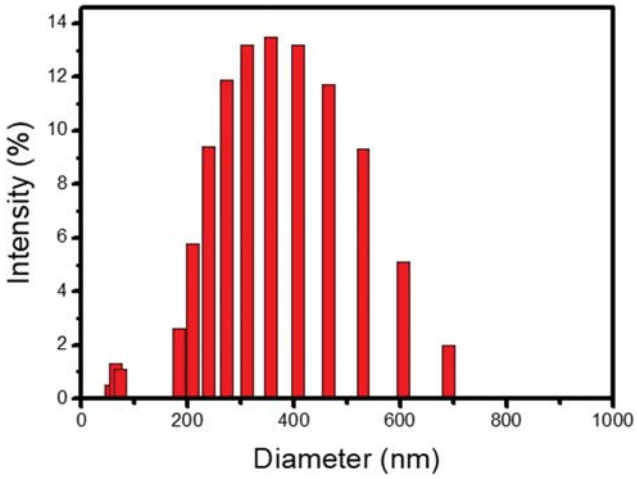

Fig. S1. Size distribution of ZnO NPs used in our study measured using DLS.

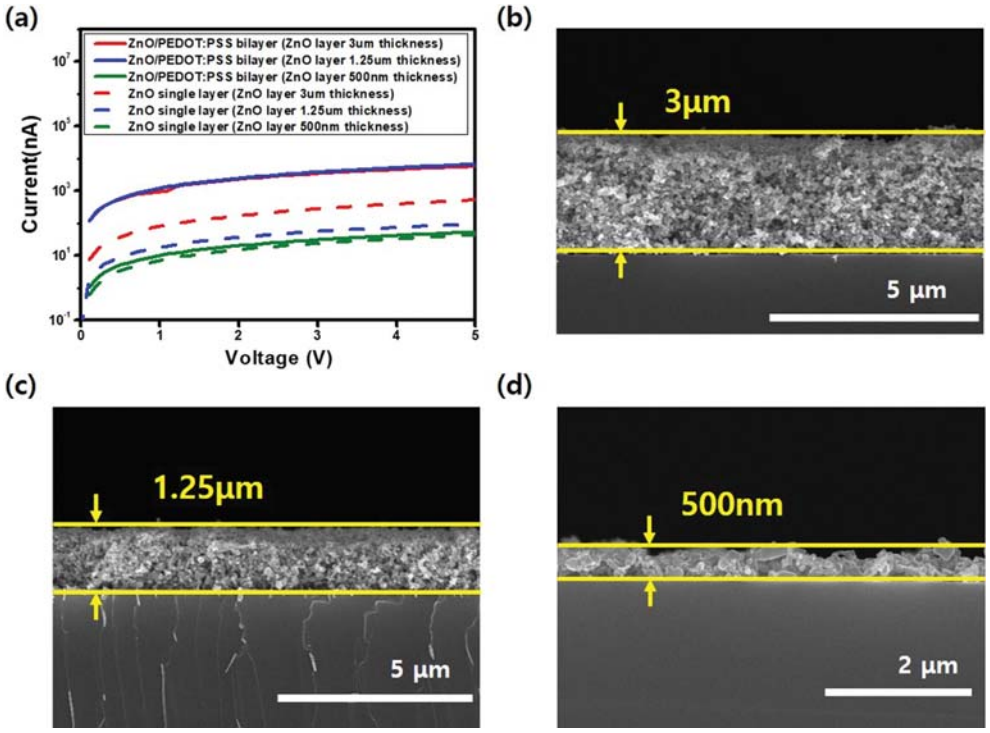

Fig. S2. (a) Current-voltage characteristics of different thickness of ZnO single layer films and ZnO/PEDOT : PSS bilayer films. Cross sectional SEM images of ZnO single layer films deposited at different thicknesses of (b) 3 μm (c) 1.25 μm, and (d) 500 nm.

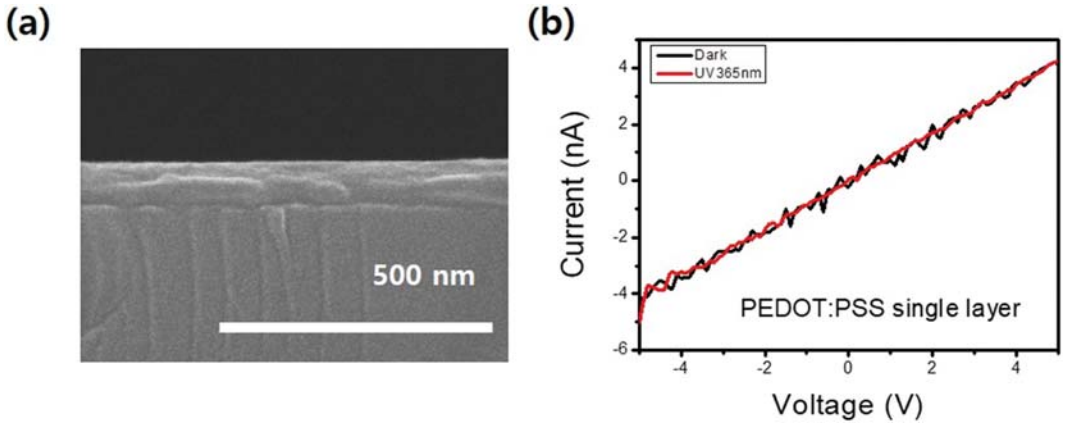

Fig. S3. (a) SEM image of PEDOT : PSS single layer and (b) I-V characteristics under 365 nm light.

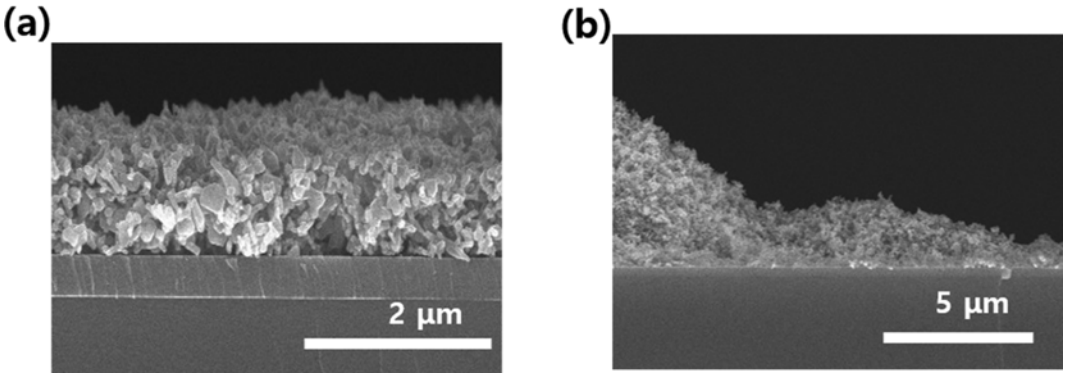

Fig. S4. Cross-sectional SEM images of ZnO single layer film deposited at different spin-coating speeds of (a) 500 rpm and (b) 300 rpm.

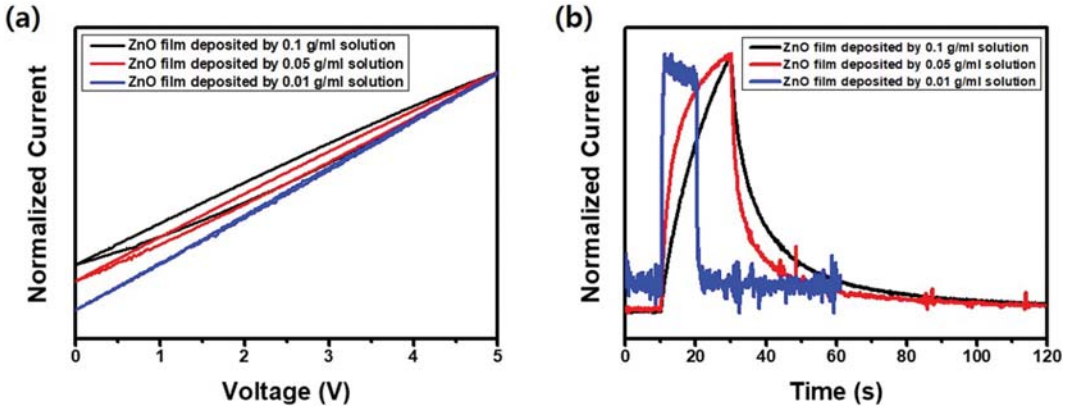

Fig. S5. (a) Cyclic I-V curve and (b) current-time characteristics of ZnO/PEDOT : PSS bilayer films with different ZnO thickness deposited by various solution conditions.